



Hepatocyte-like cells differentiated from methylmalonic aciduria *cbIB* type induced pluripotent stem cells: A platform for the evaluation of pharmacochaperoning

Á. Briso-Montiano^{a,b,c,d}, A. Vilas^{a,b,c,d}, E. Richard^{a,b,c,d}, P. Ruiz-Sala^{a,b,c,d}, E. Morato^b, L.R. Desviat^{a,b,c,d}, M. Ugarte^{a,b,c,d}, P. Rodríguez-Pombo^{a,b,c,d}, B. Pérez^{a,b,c,d,*}

^a Centro de Diagnóstico de Enfermedades Moleculares (CEDEM), Universidad Autónoma de Madrid, Cantoblanco, 28049 Madrid, Spain

^b Centro de Biología Molecular “Severo Ochoa” UAM-CSIC, Universidad Autónoma de Madrid, Cantoblanco, 28049 Madrid, Spain

^c Centro de Investigación Biomédica en Red de Enfermedades Raras (CIBERER), ISCIII, Madrid, Spain

^d Instituto de Investigación Sanitaria Hospital La Paz (IdiPAZ), ISCIII, Madrid, Spain

ARTICLE INFO

Keywords:

MMA *cbIB* type
Hepatocyte-like cells
Pharmacological chaperones
Disease cellular model
Drug evaluation

ABSTRACT

Methylmalonic aciduria *cbIB* type (MMA *cbIB* type, MMAB OMIM #251110), caused by a deficiency in the enzyme ATP:cob(I)alamin adenosyltransferase (ATR, E.C.2.5.1.17), is a severe metabolic disorder with a poor prognosis despite treatment. We recently described the potential therapeutic use of pharmacological chaperones (PCs) after increasing the residual activity of ATR in patient-derived fibroblasts. The present work reports the successful generation of hepatocyte-like cells (HLCs) differentiated from two healthy and two MMAB induced pluripotent stem cell (iPSC) lines, and the use of this platform for testing the effects of PCs. The MMAB cells produced little ATR, showed reduced residual ATR activity, and had higher concentrations of methylmalonic acid compared to healthy HLCs. Differential proteome analysis revealed the two MMAB HLCs to show reproducible differentiation, but this was not so for the healthy HLCs. Interestingly, PC treatment in combination with vitamin B₁₂ increased the amount of ATR available, and subsequently ATR activity, in both MMAB HLCs. More importantly, the treatment significantly reduced the methylmalonic acid content of both. In summary, the HLC model would appear to be an excellent candidate for the pharmacological testing of the described PCs, for analyzing the effects of new drugs, and investigating the repurposing of older drugs, before testing in animal models.

1. Introduction

Methylmalonic aciduria *cbIB* type (MMA *cbIB* type, OMIM #251110) is a recessive genetic disorder caused by a deficiency in ATP:cob(I)alamin adenosyltransferase (ATR, E.C.2.5.1.17), a mitochondrial enzyme involved in coenzyme B₁₂ metabolism. ATR catalyzes the synthesis of adenosylcobalamin (AdoCbl) from cobalamin, which involves the use of ATP. AdoCbl is the active cofactor of the mitochondrial enzyme methylmalonyl-CoA mutase (MMUT), which catalyzes the reversible isomerization of methylmalonyl-CoA to succinyl-CoA during the catabolism of branched-chain amino acids, odd-chain fatty acids, and cholesterol. MMAB (OMIM #607568) codes for ATR, a 250 amino acid protein that only becomes fully functional after adopting a

homotrimeric form [1]. The biochemical hallmark of MMA *cbIB* type is the accumulation of methylmalonic acid in plasma and urine in the absence of homocysteine [2]. Other metabolites may also be used as biomarkers of the disease; certainly, propionyl-carnitine is used in newborn screening programs [3].

Patients with MMA *cbIB* type either present with an early, severe onset form of the disease, or a milder, late onset form (2). The severe phenotype is associated with neonatal ketoacidosis, hyperlactatemia, hyperammonemia, lethargy, vomiting, failure to thrive, and hypotonia. Milder cases (usually diagnosed during infancy) are associated with failure to thrive, anorexia, vomiting and developmental delay [4]. Patients treated early may still suffer long-term complications such as acute or chronic basal ganglia injury, kidney failure, cardiomyopathy,

* Corresponding author at: Centro de Biología Molecular Severo Ochoa UAM-CSIC, Universidad Autónoma Madrid, 28049 Madrid, Spain.

E-mail addresses: a.briso-montiano@cbm.csic.es (Á. Briso-Montiano), alicia.vilas@cbm.csic.es (A. Vilas), erichard@cbm.csic.es (E. Richard), prsala@cbm.csic.es (P. Ruiz-Sala), emorato@cbm.csic.es (E. Morato), lruiz@cbm.csic.es (L.R. Desviat), mugarte@cbm.csic.es (M. Ugarte), mprodriguez@cbm.csic.es (P. Rodríguez-Pombo), bperez@cbm.csic.es (B. Pérez).

<https://doi.org/10.1016/j.bbadis.2022.166433>

Received 19 October 2021; Received in revised form 22 April 2022; Accepted 4 May 2022

Available online 13 May 2022

0925-4439/© 2022 The Authors. Published by Elsevier B.V. This is an open access article under the CC BY-NC-ND license (<http://creativecommons.org/licenses/by-nc-nd/4.0/>).

pancreatitis, and liver complications such as neoplasms [5].

Conventional treatment consists of dietary control and supplementation with hydroxocobalamin (OHCbl), N-carbamylglutamate and carnitine. Apparently, the cobalamin responsiveness observed in these patients is mutation-specific; only about 40% of patients show any such response [6,7]. Liver or liver/kidney transplantation has emerged as a means of improving biochemical outcomes and patient quality of life, but it cannot prevent the neurological damage and other clinical complications associated with the disease [8].

The mutational spectrum of patients with MMA *cblB* includes 53% missense pathogenic variants in *MMAB* (HGMD® Professional 2020.3). In a comprehensive functional analysis of missense changes described in patients, we determined the pathogenic mechanism associated with this type of variant to be a loss-of-function defect due to a reduced concentration of functional ATR. This type of loss of function mechanism has also been described for other conformational diseases [9–11]. Additionally, we reported the successful use of pharmacological chaperones (PCs, i.e., small protein-specific molecules that help normalize protein folding) to restore functional levels of originally unstable ATR. Indeed, two chemical compounds N-[(4-chlorophenyl)carbamothioyl]amino-2-phenylacetamide and 4-(4-(4-fluorophenyl)-5-methyl-1H-pyrazol-3-yl)benzene-1,3-diol (named compound V and VI, respectively), in combination with OHCbl, were able to rescue the stability, oligomerization and activity of *MMAB* destabilizing variants in a cellular model [11,12].

The next step towards the clinical use of this technology is to analyze the effects of the candidate PCs in more appropriate cellular or diseased-animal models. Cellular models generated by differentiation from induced pluripotent stem cells (iPSCs) have become enormously useful in the production of in vitro models of disease-relevant cells such as neurons, cardiomyocytes and hepatocyte-like cells (HLCs) [13]. Indeed, a number of studies have validated iPSC-differentiated models as able to reproduce disease phenotypes, and for their use as platforms for testing therapies, providing opportunities for the pursuit of personalized medicine [14].

Among the possible target organs for therapeutic drugs, the liver stands out given its size and the variety of functions it performs. Hepatocytes make up 60–80% of all liver cells, and are responsible for the organ's metabolic and secretory functions. Primary hepatocytes that maintain important metabolic phenotypes in vitro would be the best kind of cell for research purposes, but the shortage of donors and the poor expansion of these cells in culture limit their use as a platform for high-throughput drug assessment. HLCs have thus become an important preclinical model for liver pathophysiology studies and drug development, as well as a promising candidate for cell-therapy and regenerative medicine [15–18]. A range of protocols already exists for differentiating HLCs from iPSCs, all of them based on a staged process involving the use of different growth factors, beginning with the induction of endoderm [13,19].

Since no diseased-animal model is available for MMA *cblB* type, developing appropriate cellular models seems a good alternative. Hepatic models may provide an excellent option given the liver abnormalities described in patients with this disease [4,20]. The aim of the present work was to generate a diseased-liver cellular model using patient-derived iPSCs [21]. Such a model could help to investigate the use of PCs for treating defects of *MMAB*.

2. Materials and methods

2.1. Generation and characterization of MMA *cblB* hepatocyte-like cells

All the experimental protocols followed in the present study were approved by the Institutional Ethics Committee of the *Universidad Autónoma de Madrid*. Adhering to Spanish and European Union legislation, informed consent was obtained from the patients' legal guardians. Healthy CC2509 fibroblasts (Lonza, Basel, CHE) and patient-derived

fibroblasts were cultivated according to standard procedures and used before going through 20 passages. Briefly, the cells were maintained in Minimum Essential Medium (MEM) (Sigma- Aldrich, St Louis, MO, USA) supplemented with 1% (v/v) glutamine, 10% fetal bovine serum (FBS) and a 0.1% antibiotic mixture (penicillin/streptomycin) under standard cell culture conditions (37 °C, 95% relative humidity, 5% CO₂). HepG2 human hepatoma cells were grown in MEM supplemented with 5% FBS, 1% glutamine and a 0.1% antibiotic mixture under standard conditions.

Two healthy control iPSCs (C1 and C2), registered as N44SV.5 and FiPS Ctrl2-SV4F-1 respectively, were obtained from the *Banco Nacional de Líneas Celulares* of the *Instituto de Salud Carlos III*. MMA *cblB*1 iPSCs (MMAB1) and MMA *cblB*2 iPSCs (MMAB2), were reprogrammed at our laboratory from patient-derived fibroblasts as previously described [21]. These were then registered in the same cell line bank as MMAB44-FiS4F11 and MMAB35-FiS4F4, respectively. The patients who provided the fibroblasts used to generate the MMAB1 and MMAB2 cells were siblings; the provider of the latter developed late onset disease (at 4 years of age) and died shortly afterwards. In contrast, the provider of MMAB1 was diagnosed genetically before presenting symptoms [10]; indeed, the patient remains clinically asymptomatic and has apparently experienced no liver damage. Genetic analysis of fibroblasts from these siblings revealed the presence of the missense pathogenic variant c.287T>C (p.Ile96Thr) plus the loss-of-function pathogenic variant c.584G>A (r.520_584del; p.Ser174CysfsX23). [10]. Differentiation of the four iPSC lines into HLCs was achieved following a previously established protocol [19]. Briefly, 6.5×10^4 iPSCs were seeded per cm² on plates pre-coated with 5 µg·ml⁻¹ Laminin 521 (BioLamina®, Sundbyberg, Sweden). Definitive endoderm-like cells were obtained after 5 days of incubation with conditioned endoderm-priming medium (Activin A 100 ng·ml⁻¹ and Wnt3a 50 ng·ml⁻¹). Hepatic progenitor cells were obtained on day 10, after 5 more days of incubation with KSR/DMSO differentiation medium. Finally, from days 11 to 20, HLCs were obtained in culture with HepatoZYME® maturation medium supplemented with human hepatocyte growth factor (HGF 10 ng·ml⁻¹) and oncostatin M (20 ng·ml⁻¹). Every differentiation state was checked by immunofluorescence of the specific markers OCT4, SOX17, FOXA2, HNF4-alpha (HNF4α), alpha-fetoprotein (AFP), albumin (ALB) and E-cadherin.

To produce single nucleotide polymorphism (SNP) arrays, genomic DNA was isolated from MMAB1 patient-derived fibroblasts, iPSCs and HLCs by standard procedures using the MagnaPure system (Roche Applied Science, Indianapolis, IN, USA). A genome-wide scan of 850,000 SNPs was conducted at the Spanish National Genotyping Center (CEGEN) using the Illumina Infinium CytoSNP-850 K Beadchip SYSTEM according to the manufacturer's recommendations (Illumina, San Diego, CA, USA). DNA was quantified using Picogreen (Invitrogen, Waltham, MA, USA) and genomic profiles created using Illumina GenomeStudio 2.0 software, which plots SNP data over the chromosomes. The log R ratio of signal intensities was determined as the log (base 2) ratio of the observed intensity value versus the expected intensity for an SNP, divided by the expected normalized R value.

For gene expression analysis, cDNA was obtained using 500 ng of total RNA from healthy (CC2509) and from patient-derived fibroblasts, C1 and C2 healthy control iPSCs, MMAB1 and MMAB2 iPSCs, HepG2, and all four HLCs (C1, C2, MMAB1 and MMAB2), before and after PC treatment. First strand cDNA was obtained using the NZY First-Strand cDNA Synthesis Kit (NZYtech, Lisbon, Portugal) for the quantification of *GAPDH*, *SOX17*, *FOXA2*, *HNF4a*, *AFP*, *ALB*, *PCCA*, *PAH*, *OTC*, *SERPIN1A1*, *ORM1*, *HP*, *AMBP* and *MMAB*, which were amplified with specific primers (available upon request). Quantification was performed using the 2^{-ΔΔCt} method, employing the Perfecta SYBR Green FastMix Kit (QuantaBio, Beverly, MA, USA) in a LightCycler480 II instrument (Roche Applied Biosciences). *GAPDH* was used as an endogenous control.

For immunofluorescence assays, iPSCs were grown over Laminin 521 on µ-Slide 8 Well culture plates (Ibidi, Gräfelfing, Germany) and fixed

with a 10% formalin solution (Sigma-Aldrich, St Louis, MO, USA). The antibodies used were those against MMAB (ProteinTech, Rosemont, IL, USA; 1:200), ATP5a (Abcam, Cambridge, UK; 1:200), OCT4 (Santa Cruz Biotechnology, Dallas, TX, USA, 1:60), SOX17 (Santa Cruz Biotechnology; 1:200), FOXA2 (Santa Cruz Biotechnology, 1:200), HNF4 α (Santa Cruz Biotechnology, 1:100), AFP (Santa Cruz Biotechnology, 1:50), ALB (Cedarlane, Burlington, Ontario, Canada; 1:50) and E-Cadherin (Cell Signaling, Danvers, MA, USA; 1:200). The secondary antibodies used (1:200) were from Jackson Immunoresearch (Philadelphia, PA, USA) and Thermo Fisher Scientific (Waltham, MA, USA). DAPI (Invitrogen, Waltham MA, USA; 1:10,000) was used to stain nuclei. Images were taken using a Zeiss confocal microscope. For the assessment of PC treatment, images were taken after 72 h of incubation and the intensity of fluorescence analyzed using Fiji software.

For western blot analysis, 30 or 75 μ g total protein from crude extracts from C1, C2, MMAB1 and MMAB2 HLCs were loaded onto NuPage \textregistered 4–12% Bis-Tris gel (Life Technologies, Waltham MA, USA). After SDS-PAGE, the proteins were transferred to nitrocellulose membranes using the iBlot Transfer Device (Life Technologies). Ponceau staining was used to ensure equality in protein loading. Immunodetection was performed using the commercially available primary antibody anti-MMAB (ProteinTech; 1:1000); goat-anti rabbit IgG coupled with horseradish peroxidase was used as the secondary antibody (Cell Signaling, 1:5000). Detection was performed using the Enhanced Chemiluminescence System (GE Healthcare, Chicago, IL, USA). The same was performed for ornithine transcarbamylase (OTC) and alpha (1)-acid glycoprotein (AGP) detection using Abcam antibodies (1:1000), for haptoglobin (HP) and alpha-1-microglobulin/bikunin precursor (AMBp) detection using Thermo Fisher Scientific antibodies (1:1000 and 1:500, respectively), and for AFP detection using Santa Cruz Biotechnology antibodies (1:500), for phenylalanine hydroxylase (PAH) using Cell Signaling antibodies (1:2000), for PCCA using Santa Cruz Biotechnology antibodies (1:1000), for α -1-antitrypsin (AAT) using Santa Cruz Biotechnology antibodies (1:500), and for ALB using Cedarlane antibodies (1:500). The blots were stripped and reprobed with Abcam anti-GAPDH antibodies (1:5000) as a loading control. Relative protein quantities were determined using a calibrated GS-800 densitometer (BioRad, Hercules, CA, USA).

2.2. Proteomic analysis of differentiated HLCs

Soluble extracts of C1 and MMAB1 HLCs, treated or untreated with PCs, were digested as previously reported [22] (performed in duplicate). Briefly, after protein denaturation with 8 M urea in 50 mM ammonium bicarbonate pH 8.8, samples were reduced and alkylated with 10 mM DTT for 1 h at 37 °C, and 10 mM iodoacetamide for 30 min at room temperature in darkness, respectively. The samples were then diluted to reduce the urea concentration below 1.4 M and digested using sequencing grade trypsin (Promega, Madison, WI, USA) overnight at 37 °C using a 1:20 (w/w) enzyme:protein ratio. Digestion was stopped by the addition of 1% TFA. Whole supernatants were dried down and then desalted onto OMIX Pipette tips C18 (Agilent Technologies, Santa Clara, CA). The resultant peptide mixture (80 μ g) was labeled using chemicals from the TMT 6-plex Isobaric Mass Tagging Kit (Thermo Fisher Scientific) essentially as described by the manufacturer. Samples were mixed and analyzed by reverse phase-liquid chromatography (RP-LC-MS/MS) to check the efficiency of labeling [23]. The samples were then fractionated using the Pierce High pH Reversed-Phase Peptide Fractionation Kit (Thermo Fisher Scientific), and the fractions analyzed by RP-LC-MS/MS in an Easy-nLC II system coupled to an ion trap LTQ-Orbitrap-Velos-Pro hybrid mass spectrometer (Thermo Fisher Scientific) as previously described [24].

Peptide identification from raw data was performed using the PEAKS Studio X Pro search engine (Bioinformatics Solutions Inc., Waterloo, Ontario, CAN) and the uniprot-homo-sapines.fasta database (74,811 entries; Uniprot release 12/2019), employing the following constraints:

tryptic cleavage after Arg and Lys (semi-specific), up to two missed cleavage sites, a tolerance of 20 ppm for precursor ions, and of 0.05 Da for MS/MS fragment ions. Searches were performed allowing for optional Met oxidation and Cys carbamidomethylation, and for fixed TMT 6plex reagent labeling the N-terminus and lysine residues [23]. False discovery rates for peptide spectrum matches and for protein were limited to 1%. Only those proteins with at least two unique peptides discovered by LC/MS/MS were considered reliably identified and thus quantified.

TMT-labeled peptides were quantified using the PEAKS Studio X Pro search engine, with “Reporter Ion Quantification iTRAQ/TMT” selected under the “Quantifications” options. The auto-normalization mode was used; this calculates a global ratio from the total intensity of all labels for all quantifiable peptides. For protein quantification, only unique peptides were taken into account; protein groups identified as having the same peptides were considered as one entry in peptide analyses; isoforms were not included. Finally, for protein categorization, in silico analysis was performed based on gene ontology enrichment with STRING (<https://string-db.org/>), Reactome (<https://reactome.org/>) and KEGG pathway (<https://www.genome.jp/kegg/>) database support. 105 proteins associated with the hepatic phenotype were selected from the literature [25] and GTEx Portal database (liver, <https://gtexportal.org/home/eqtls/tissue?tissueName=Liver>).

2.3. Biochemical characterization of hepatocyte like-cells and assessment of chaperone treatment

ATR activity was assessed in C1 and MMAB1 HLCs by measuring the incorporation of [14 C]-propionate into precipitable protein extracts before and after PC treatment. At day 20 of iPSC differentiation, HLCs were maintained in conditioned HepatoZYME \textregistered medium and incubated with 1 μ g·ml $^{-1}$ OHCbl alone or in combination with compound V (N-[(4-chlorophenyl) carbamothioyl]amino)-2-phenylacetamide, 80-or-250 μ M) or compound VI (4-(4-(4-fluorophenyl)-5-methyl-1H-pyrazol-3-yl)benzene-1,3-diol, 5 μ M) for 72 h. DMSO (0.2%) was used as a negative control. The cells were then incubated at 37 °C for 18 h in the presence of [14 C]-propionate, harvested by trypsinization, microcentrifuged for 5 min at maximum speed, and used to determine ATR activity - indirectly measured via the incorporation of [14 C]-propionate (1 μ Ci·ml $^{-1}$) into acid-precipitable proteins [11]. Radioactivity was quantified as counts per minute, as measured with a radiometric counter (PerkinElmer, Waltham, MA, USA).

After 72 h, cell medium from HLC culture was collected and stored at 4 °C for organic acid determinations. The supernatant was used for MMA quantification by liquid chromatography coupled to tandem mass spectrometry (HPLC/MS/MS), without derivatization, employing stable isotope-labeled MMA as an internal standard [26]. The protein concentration was determined by the Bradford method for sample normalization (μ mol MMA · μ g $^{-1}$ protein).

Finally, cytotoxicity assays were performed using the CellTiter 96 \textregistered Aqueous One Solution Cell Proliferation Kit (Promega) in 96-well plates following the manufacturer's instructions. MMAB1 iPSCs were differentiated into HCLs in 96-well plates, and after 20 days the latter were treated with PCs and incubated for 72 h. Different combinations of compounds were used: a previously effective PC treatment [9], i.e., 80 μ M V + 5 μ M VI + 1 μ g·ml $^{-1}$ OHCbl named treatment 1 (T1); a new combination, i.e., 250 μ M V + 5 μ M VI + 1 μ g·ml $^{-1}$ OHCbl. named treatment 2 (T2); and a third new combination, i.e., 250 μ M V + 1 μ g·ml $^{-1}$ OHCbl named treatment 3 (T3). OHCbl and DMSO were used as controls.

2.4. Statistics

Data are reported as the mean \pm standard deviation. qPCR data correspond to only one HLC differentiation replicate. Data were analyzed by one-way ANOVA (followed by the Bonferroni post hoc test)

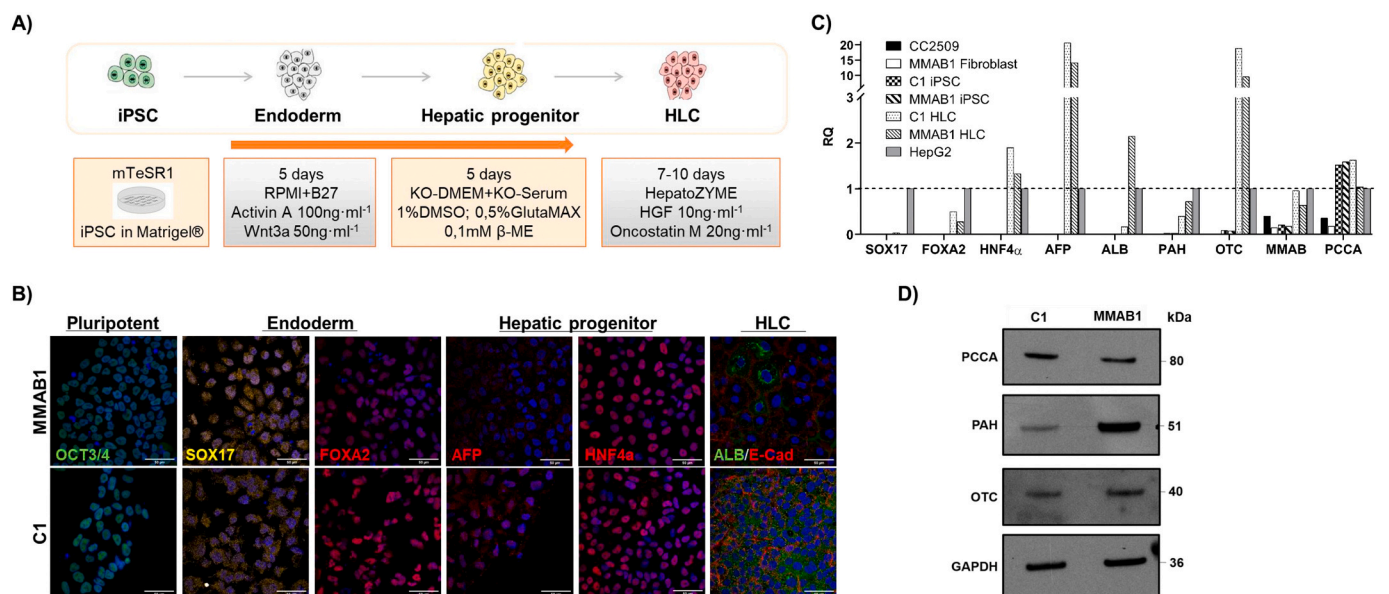


Fig. 1. iPSC differentiation into hepatic-like cells (HLC): **A.** Diagram showing the differentiation of healthy and patient iPSCs into HLCs. iPSCs were incubated sequentially with culture media containing specific growth factors as previously described [24]. **B.** Immunofluorescence of specific markers to check for the different steps of differentiation in C1 and MMAB1 HLCs. All images were taken with a 40× objective; scale bar 50 μm. **C.** Relative expression of genes related to differentiation (SOX17, FOXA2, HNF4α, AFP), specific hepatic proteins (ALB, PAH, OTC), and proteins involved in the propionate degradation pathway (MMAB, PCCA). RT-qPCR was performed using cDNA from healthy CC2509 and MMAB1 patient-derived fibroblasts, C1 and MMAB1 iPSCs, C1 and MMAB1 HLCs, and HepG2 cells. The fold change is compared to HepG2 (dashed line = 1). **D.** Western blot of liver-specific proteins such as OTC, PAH and PCCA from C1 and MMAB1 HLC soluble lysates. GAPDH was used as a loading control.

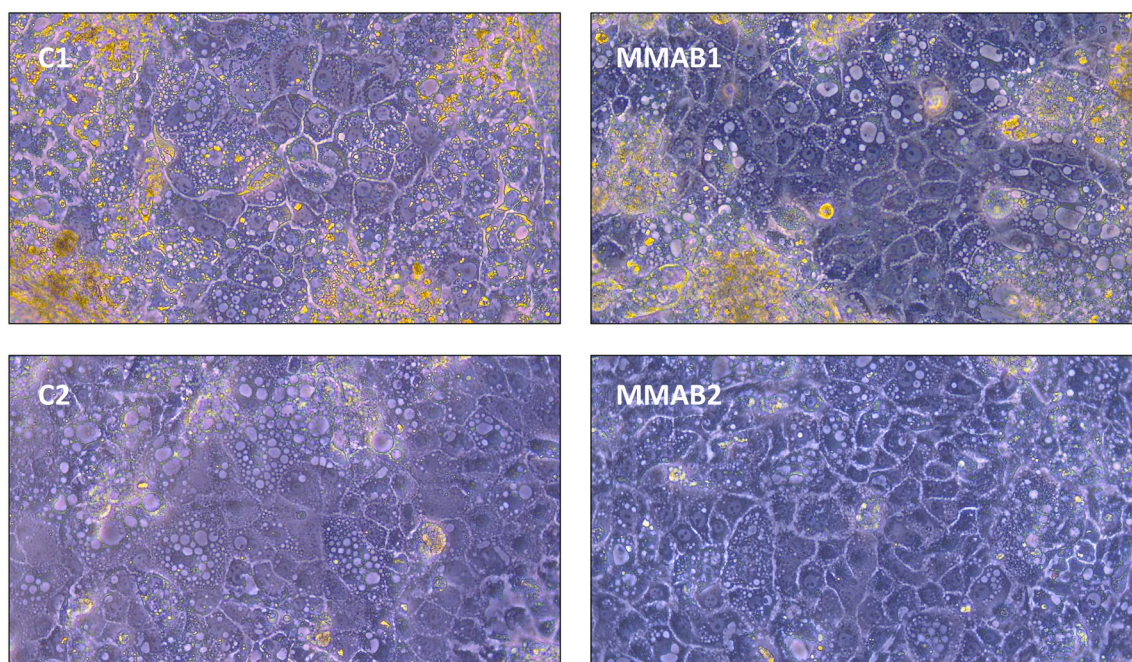


Fig. 2. Hepatocyte-like cell morphology after differentiation. Representative bright field microscopy images of C1, C2, MMAB1 and MMAB2 HLCs at day 22 of differentiation. Images taken with 20× objective.

or the student *t*-test as required, using IBM SPSS Statistics software for Windows.

3. Results

3.1. Generation and evaluation of diseased hepatocyte-like cells

The generation of the healthy and MMAB HLC models was performed

by multistage differentiation cascade from the endoderm layer, using different factors as previously described [19] (Fig. 1A). Differentiation was monitored by immunofluorescence detection of specific pluripotent (OCT3/4), endodermal (SOX17 and FOXA2), or fetal hepatocyte nuclear factor 4-alpha (HNF4α). At the beginning of the process, cells expressed OCT3/4 as a pluripotency marker; after 5 days in the presence of activin A and Wnt3a, the markers of definitive endoderm FOXA2 and SOX17 were detected. After five more days, the expression of alpha-fetoprotein

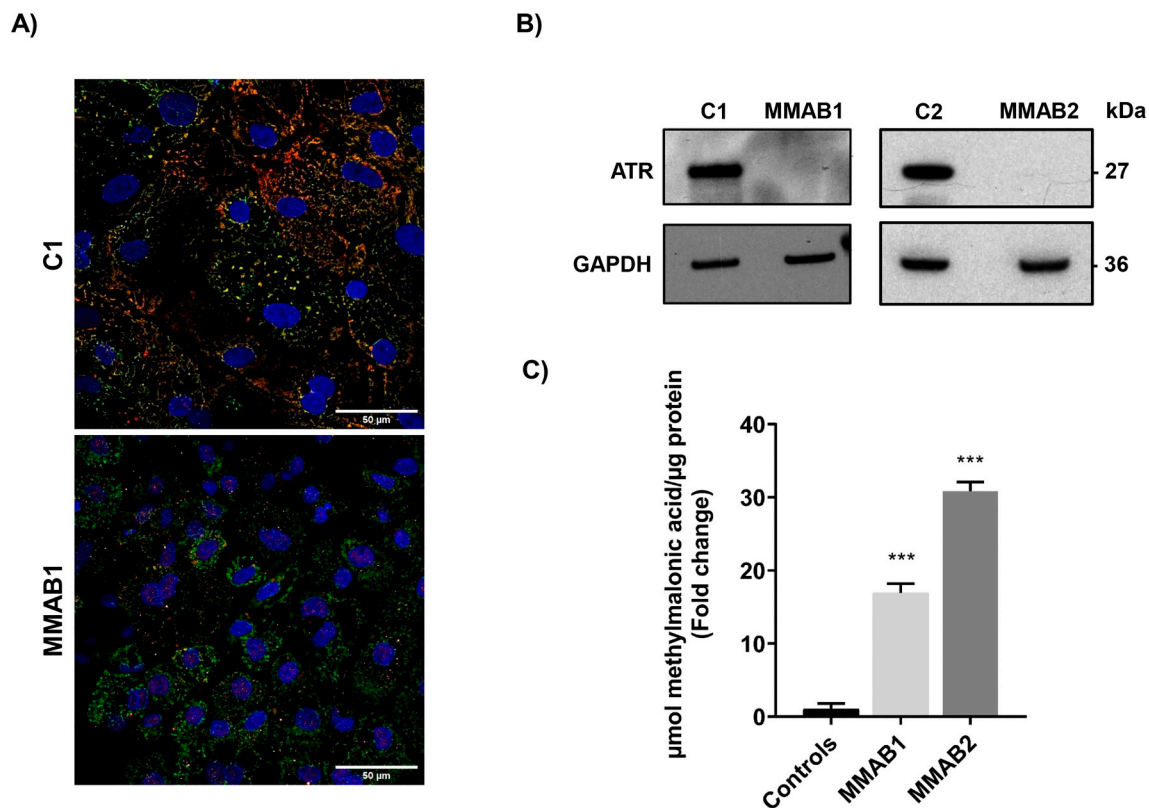


Fig. 3. Disease biomarkers in differentiated control and MMAB HLCs. **A.** Immunofluorescent detection of ATR (red) and the mitochondrial protein ATP5a (green) in C1 and MMAB1 HLCs (40× objective; scale bar 50 μm). The image shows the co-localization of both proteins in the mitochondria. **B.** Western blot immunodetection of ATR in C1, C2, MMAB1 and MMAB2 HLCs. GAPDH was used as a loading control. **C.** Quantification of methylmalonic acid in spent culture medium from healthy controls (mean of C1 and C2 methylmalonic acid levels) and diseased (MMAB1 and MMAB2) HLCs, with respect to the protein concentration in each corresponding sample. Values are fold changes with respect to controls. Differences were analyzed using the Student *t*-test (***) $p < 0.001$. (For interpretation of the references to colour in this figure legend, the reader is referred to the web version of this article.)

(AFP) and HNF4α was observed, indicating an embryonic hepatic state. Differentiation into a hepatic lineage was also observed morphologically (Fig. 2).

On day 20, HLCs were obtained in response to incubation with hepatocyte growth factor and oncostatin M. The final step of HLC differentiation involved the immunodetection of ALB and E-cad (Fig. 1B). The variants in *MMAB* shown by the patients were present in the HLCs; no large rearrangements were detected by SNP array analysis.

Once the C1 and MMAB1 HLCs were generated, specific hepatic markers and metabolic enzymes were analyzed by RT-qPCR (Fig. 1C) and western blotting (Fig. 1D). Compared to HepG2 cells (commonly used as a hepatic lineage), the HLCs expressed increased mRNA levels for the hepatic markers *AFP* and *HNF4α*. The expression of *ALB* was observed in all the HLCs, with the strongest seen in the MMAB1 HLCs, along with the liver enzyme genes *PAH* and *OTC* (Fig. 1C). The HLCs expressed the highest levels of *OTC*, while the HepG2 cells showed stronger *PAH* expression. No expression of any of these hepatic protein genes was observed in the healthy or patient-derived fibroblasts, or iPSCs. Although *MMAB* and α-subunit propionyl-CoA carboxylase (*PCCA*) are expressed ubiquitously, they are not present at the same amounts in all cells and tissues. Indeed, *MMAB* and *PCCA* mRNAs were expressed at similar or slightly higher levels in the HLCs (C1 and MMAB1) than in HepG2 cells, but at clearly higher levels than in the corresponding healthy and patient-derived fibroblasts. The levels of *MMAB* mRNA were lower in patient-derived cells than healthy cells due to the effect of the p.Ser174CysfsX23 variant (Fig. 1C). No significant differences in *PCCA* expression were observed between iPSCs and HLCs.

ATR was detected by western blotting and immunofluorescence, co-localized with the mitochondrial protein ATP5a. The

immunofluorescence results showed a significant reduction in ATR in MMAB1 HLCs compared to C1 HLCs (Fig. 3A). Similarly, western blotting detected no ATR protein in any of the *MMA cblB*-type HLCs (Fig. 3B). Determining the concentration of methylmalonic acid in spent culture medium by mass spectrometry revealed increased levels of methylmalonic acid in MMAB1 and MMAB2 HLCs (0.46 ± 0.03 and 0.51 ± 0.02 μmol MMA-L⁻¹ respectively) - 17 and 31 times higher respectively than the mean for the control HLC culture medium after normalization against the protein concentration (Fig. 3C).

To elucidate the molecular pathways altered in *MMA cblB* type, and to assess the effect of the candidate PCs, the proteome signatures of the C1 and MMAB 1 HLCs were examined (Fig. 4). The reliability of HLC generation is shown by the heat map overview (Fig. 4A and B). Forty-four specific liver-expressed proteins listed in the GTEx Portal database were detected, but neither the cytochrome P450 nor phase I/II metabolic enzymes produced by mature hepatocytes appeared to be present.

The MMAB1 HLC proteome expression profile was compared to that of the C1 healthy HLC proteome to identify differentially expressed proteins (DEPs). Ninety significantly dysregulated proteins were detected in the former HLCs, of which 42 were upregulated and 48 down-regulated (Supplementary Table 1). Three main subnetworks involving these 90 proteins were revealed through the use of the STRING database. The dysregulated proteins were clustered into seven physiological systems reflecting different biological processes (Supplementary Table 1). Three main nodes corresponding to the proteostasis network, metabolism, and the inflammation pathway (Supplementary Fig. 1), were then focused upon. Table 2 shows that some liver proteins were upregulated.

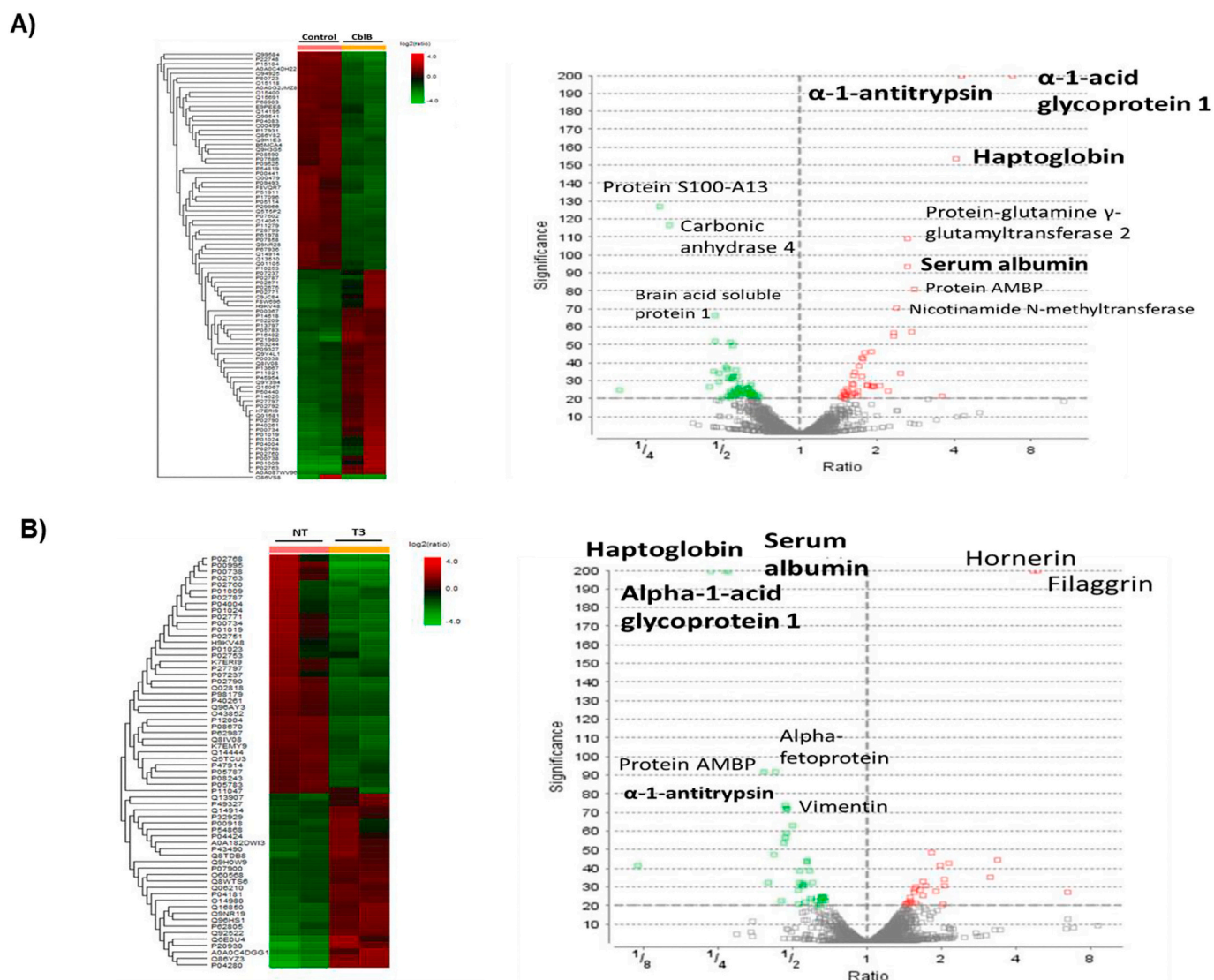


Fig. 4. Proteome analysis before and after PC treatment. A and B. Heat map and volcano plot of proteome profiles for duplicates of the C1 HLC proteome (first two columns) compared to the MMAB1 HLC proteome (two last columns) (A), and the MMAB1 HLC proteome (NT) compared to the T3-treated MMAB1 HLC proteome (B). Up-regulated proteins appear as red bars, and down-regulated proteins as green bars. Some DEPs are labeled and highlighted. Y-axis: significance score is calculated as the $-10\log_{10}$ of the significance testing p -value. (For interpretation of the references to colour in this figure legend, the reader is referred to the web version of this article.)

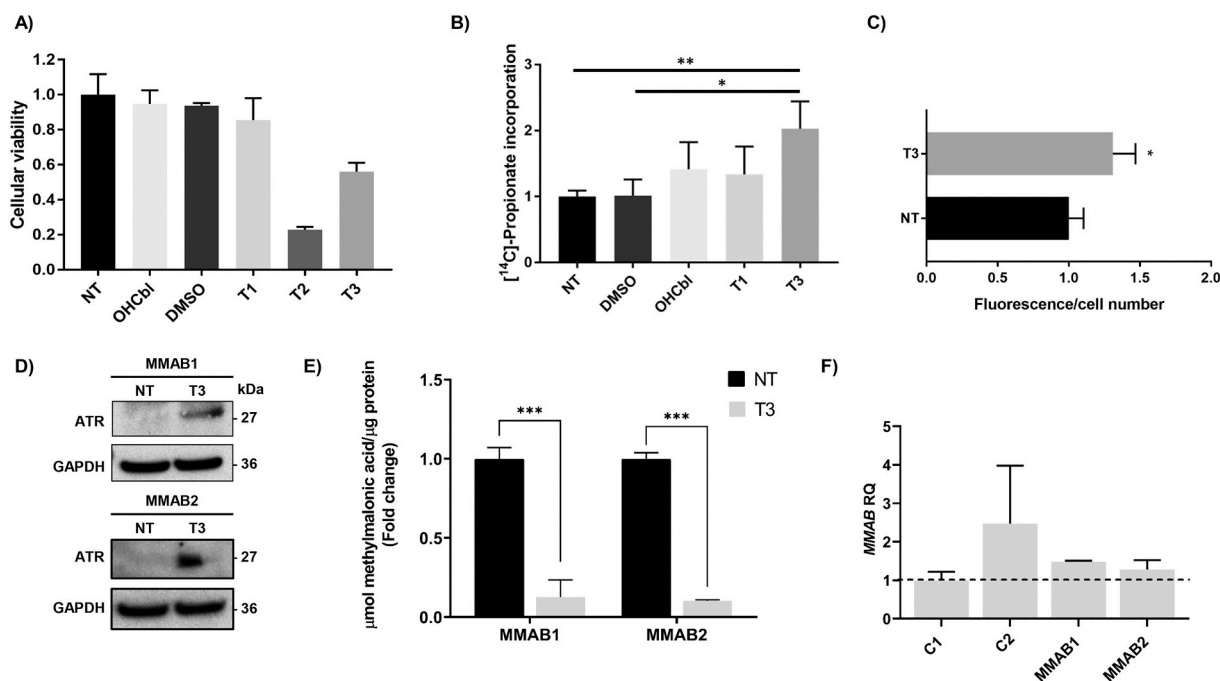
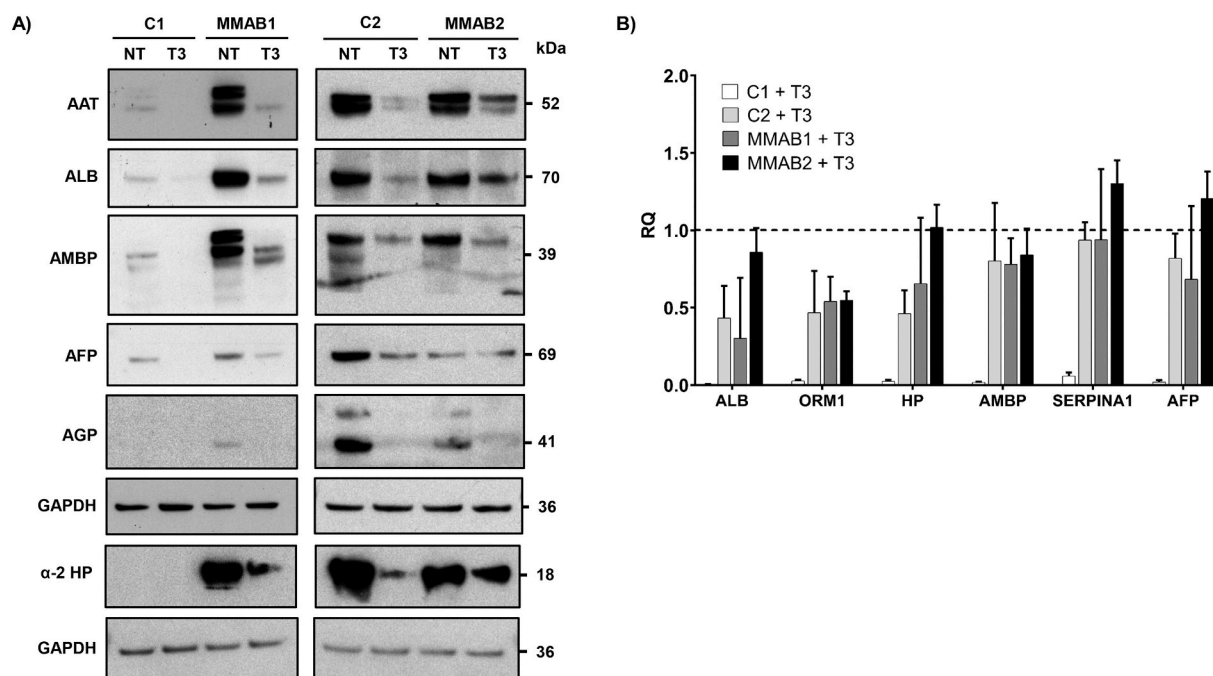
To confirm the differential expression of proteins, a number of hepatic proteins were analyzed in the C1, C2, MMAB1 and MMAB2 HLCs by western blotting and RT-qPCR. The analysis of proteins obtained in a second C1 and MMAB1 HLC differentiation confirmed the results obtained in the untargeted differential proteomics analysis, with larger amounts of all the studied proteins detected in the MMAB1 HLCs than in the C1 HLCs (Fig. 5A). Nevertheless, qualitative proteome analysis by western blotting of C2 HLCs showed similar amounts of AAT, ALB, AMBP, and α -2HP, and a slightly larger amount of AFP and AGP compared to that seen for the MMAB1 or MMAB2 HLCs. These results suggest inter-line variability in terms of C1 and C2 HLC differentiation, while the levels of proteins examined were similar in the MMAB1 and MMAB2 HLCs.

3.2. Pharmacological chaperone treatment

The effects of compounds V and VI were examined in MMAB1 HLCs. Cells were incubated for 72 h at 37 °C in the presence of different combinations and concentrations of compounds V, VI and OHCbl.

Cytotoxicity was determined first with three combinations (Fig. 6A), and after this their effect on the activity of the propionate pathway was investigated. Treatment T1 was the most effective combination in patient-derived fibroblasts [11], but it did not significantly increase ATR activity in MMAB1 HLCs (Fig. 6B). Higher concentrations of compounds V and VI were therefore tried (T2), as was an additional treatment without compound VI (T3) (due to its high cytotoxicity). The T3 treatment increased ATR activity to twice that of the basal condition (Fig. 6B). The detection of the ATR protein by immunofluorescence also revealed a significant increase in the T3-treated MMAB1 HLCs compared to the non-treated control C1 HLCs (Fig. 6C). Western blotting detected ATR only in the T3-treated MMAB1 and MMAB2 HLCs (Fig. 6D). Further, the T3 treatment reduced the methylmalonic acid levels in the spent culture medium for both the MMAB1 and MMAB2 HLCs by more than 85% (as determined by mass spectrometry) (Fig. 6E). The MMAB mRNA levels slightly increased after T3 treatment, especially in the C2 HLCs (Fig. 6F).

The effect of T3 on the proteome signature was then determined, comparing treated and untreated MMAB1 HLCs (Fig. 4B). Only 61



significantly dysregulated proteins were detected in the treated cells, of which 25 were upregulated and 36 downregulated (Supplementary Table 1). Some proteins related to liver damage and inflammation were reduced after treatment (Table 2).

To examine the effect of T3 on liver hepatic proteins on the 20th day of differentiation, expression levels were analyzed in the C1, C2, MMAB1 and MMAB2 HLCs after 72 h of treatment. Surprisingly, the T3 treatment seemed to contribute to reductions in all the studied proteins in all cells, except for AFP in the MMAB2 HLCs (Fig. 5). This reduction was most evident in the C2 HLCs. The levels of all mRNAs tested were similar to or reduced compared to those recorded for untreated cells, except for those of *SERPINA1* and *AFP* in the MMAB2 HLCs which remained slightly increased (as detected for *AFP*).

4. Discussion

MMA *cblB* type is mostly the result of a reduction in ATR caused by destabilizing variants [10,11]. In earlier work we described the first proof-of-concept for the use of PCs as a therapeutic option for many patients with MMA *cblB* type [11,12]. An important step in bringing PC treatment to the bedside is, however, the generation of an appropriate disease model for testing the effects of candidate compounds before preclinical testing in a diseased-animal model. In the present work, a hepatic cellular model was generated that could be used as a platform for drug testing.

Reprogramming patient-derived fibroblasts into iPSCs, and differentiating them into specific cell types, allows therapies for use in specific genetic backgrounds to be developed [33]. The generation of HLCs using iPSC technology may be useful in screening for drug toxicity, basic research, and in the development of liver transplantation technologies [34]. Our group previously generated two MMAB iPSC lines from patient-derived fibroblasts [21]. In the present work, the MMAB HLCs differentiated from these iPSCs exhibited the hepatic proteins ALB, alpha-1-antitrypsin (AAT), PAH and OTC that are lacking in iPSCs and patient-derived fibroblasts. The mRNA levels and common liver proteins detected by proteome analysis indicate the similar stage of differentiation reached by the MMAB1 and MMAB2 HLCs (both have a similar genetic background). However, the C1 and C2 HLCs showed evidence of being at different stages of differentiation. The multistage differentiation cascade promotes the acquisition of sequentially specific biomarkers; the HLCs generated are like fetal or newborn hepatocytes [25], and the degree of differentiation of different healthy controls is likely diverse. For tissue therapy, however, the challenge is to achieve hepatocyte maturation by increasing the time of exposure to hepatic growth factors, or using 3D culture techniques [34].

The present model could be used as a drug evaluation platform. The MMAB HLCs have all the biochemical and molecular hallmarks of the disease. Indeed, they showed reduced mitochondrial ATR compared to the healthy control HLC lines, as well as reduced ATR activity and significantly increased methylmalonic acid levels. This work thus represents an advance in the unlimited generation of diseased HLCs, and provides a platform for drug discovery, plus a starting point for the development of liver organoids and cell-based corrective therapies [34,35]. These results also open an avenue for the use of PCs in rescuing ATR activity. Further, the determination of methylmalonic acid in the spent HLC culture medium by mass spectrometry supports the use of this model for drug repurposing research, or the discovery of new drugs, before moving on to testing in animal models. The treatment-induced reductions in mRNA levels for all the examined proteins in almost all control and patient-derived HLCs needs further investigation, as does the never-before described upregulation of *MMAB* in HLCs.

The HLC model was here used to test the effectiveness of selected PCs [11,12]. Different combinations of PCs were tested to identify the most effective treatment as previously reported [11]. The results suggest compound VI to be highly toxic in HLCs; before further testing it should be chemically modified. Overall, the results showed that the

combination of compound V and OHcbl could go on to be tested in animal models. This treatment increased the concentration of ATR that seen in non-treated MMAB HLCs by up to five times, doubled the ATR activity, and reduced methylmalonic acid levels by more than 85% in both MMAB HLCs. An increase in *MMAB* mRNA levels was also detected, suggesting the transcriptional activation of this gene. Experiments are underway to examine this further.

Proteome differential expression analysis suggested three main networks to be dysregulated: metabolism, proteostasis, and liver inflammation. For the metabolism system, an enrichment in proteins involved in lipid, amino acid and glucose metabolism was seen (Supplementary Fig. 1). In particular, two flavoproteins were upregulated: 1) the mitochondrial short-branched chain-specific acyl-CoA dehydrogenase related to 3-methylbutyryl-CoA in the isoleucine catabolic pathway, but which is also able to react with other 2-methyl branched-chain substrates and with short straight chain acyl-CoAs [36], and 2) peroxisomal acyl-CoA oxidase 1, a representative enzyme of fatty acid β -oxidation found mainly in eukaryote peroxisomes [37]. Cytoplasmic hydroxymethylglutaryl-CoA synthase (HMG-CS1) involved in cholesterol synthesis was also upregulated. The upregulation of pyruvate kinase and L-lactate dehydrogenase A, involved in glucose metabolism, was also noted. So too was that of mitochondrial glutamate dehydrogenase 1 (GLUD1), an enzyme involved in glutamate degradation for α -ketoglutarate synthesis (the precursor of succinyl-CoA in the tricarboxylic acid cycle, made in response to elevated ADP/ATP ratio or low levels of succinyl-CoA) [38]. Indeed, 2D-DIGE proteomic analysis of liver specimens from donors and patients with MMA has detected impaired hepatic metabolism [39] with important perturbations in the enzymes involved in energy metabolism, gluconeogenesis and Krebs cycle anaplerosis. The present data, obtained by LC/MS-MS, support the differential expression of specific proteins involved in intermediary metabolism.

It is important to understand the metabolic adaptations caused by the lack of Krebs cycle intermediates [39]. In this respect, the described upregulation of glutamate dehydrogenase (GLUD1) in the latter work may well be related to the hyperammonemia experienced by patients with MMA. This enzyme was also detected as being upregulated in the present proteome analysis, but levels were corrected by the T3 treatment. The targeted inhibition of GLUD1 has been suggested as a potential way of treating hyperammonemia in MMA [39], which the present results appear to support.

The proteome profile also revealed the dysregulation of 15 proteins related to inflammation and the innate acute phase immune response (APR) [40,41]. Among the APR proteins, important anti-inflammatory proteins were seen to be increased, including α -1-acid glycoprotein and α -1-antitrypsin (involved in the regulation of local inflammation [35–38]) and haptoglobin (an inflammatory regulator related to systemic inflammation and oxidative stress in other diseases [46]). Within this APR group were proteins with no pro-inflammatory effects such as fibrinogen and complement C3 [47]. Other significantly dysregulated proteins that do not belong to the APR group, but are involved in this pathway, included prostaglandin reductase (involved in pro-inflammatory leukotrien-B4 inactivation [48]) and annexin 1 [49]. In addition, a number of genes related to lysosomal activity, intracellular trafficking, morphology and cellular structure were found to be downregulated in the disease model HLCs (see Supplementary Table 1). Indeed, the *CblB* proteome showed clearly reduced lysosomal activity, highlighted by the downregulation of lysosomal enzymes such as cathepsin B [50], β -hexosaminidase, lysosomal alpha-glucosidase, acid ceramidase and granulin, all of which are involved in the control of lysosomal acidification [51]. Lower levels of intracellular trafficking members such as SNARE proteins, syntaxin 12 and 7, and hook3, were also detected [52]. These DEPs might be related to the downregulation of most proteins involved in the organization and maintenance of the cell structure recently reported in a methylmalonic aciduria MMUT type model generated by CRISPR/Cas9 editing [53]. The *CblB*-HLC proteome

Table 1

Dysregulated expression proteins before and after pharmacochaperoning treatment.

Ontology ID process ¹	Protein name (Uniprot ID)	UP/DOWN (Fold value) ^{1, 2 and 3}		Cell localization
		No treatment	PC treatment	
Proteostasis ³				
Protein folding (GO:0006457)	Protein disulfide-isomerase (P07237)	UP (1.51)	DOWN (0.66)	ER, EN
	Calreticulin (P27797)	UP (1.75)	DOWN (0.57)	ER, EN
	Endoplasmic reticulum chaperone BiP (P11021)	UP (1.69)	–	ER, EN
	Protein disulfide-isomerase A4 (P13667)	UP (1.64)	–	ER, EN
	Heat shock protein HSP 90-alpha (P07900)	UP (1.54)	–	ER, EN
	Hypoxia up-regulated protein 1 (Q9Y4L1)	–	UP (1.49)	ER, EN
Endoplasmic reticulum unfolded protein response (GO:0030968)		UP (1.49)	–	ER
Translational elongation (GO:0006414)	Receptor of activated protein C kinase 1 (P63244)	UP (1.52)	–	C, N, PM
Proteolysis involved in cellular protein catabolic process (GO:0051603)	Probable serine carboxypeptidase CPVL (Q9H3G5)	DOWN (0.59)	–	ER, S
Protein binding (GO:0005515)	Peptidyl-prolyl cis-trans isomerase FKBP10 (Q96AY3)	–	DOWN (0.66)	ER, EN
Protein ubiquitination (GO:0016567)	Ubiquitin-60S ribosomal protein L40 (P62987)	–	DOWN (0.52)	ER, C
Metabolism				
Lipid metabolic process (GO:0006629)	Peroxisomal acyl-coenzyme A oxidase 1 (Q15067)	UP (1.83)	–	M
	Hydroxymethylglutaryl-CoA synthase cytoplasmic (Q01581)	UP (2.05)	–	C
	Apolipoprotein A-I (P02647)	UP (1.94)	–	C, S
	Apolipoprotein C-I (P02654)	UP (1.9)	DOWN (0.56)	S
	NPC intracellular cholesterol transporter 1 (O15118)	DOWN (0.48)	–	N
	Fatty acid synthase (P49327)	–	UP (1.44)	C, PM
	Hydroxymethylglutaryl-CoA synthase (P54868)	–	UP (1.5)	M
	Isopentenyl-diphosphate Delta-isomerase 1 (Q13907)	–	UP (1.64)	P
	Acetyl-coenzyme A synthetase (Q9NR19)	–	UP (2.04)	C
	Short/branched chain specific acyl-CoA dehydrogenase mitochondrial (P45954)	UP (1.65)	–	M
Carboxylic acid metabolic process (GO:0019752)	Glutamate dehydrogenase 1 mitochondrial (P00367)	UP (1.44)	–	M
	Glutaminase kidney isoform mitochondrial (O94925)	DOWN (0.48)	–	M
	Glycine amidinotransferase mitochondrial (P50440)	UP (1.84)	–	M
	Glutamine synthetase (P15104)	DOWN (0.46)	–	C, M
	Pyruvate kinase PKM (P14618)	UP (1.48)	–	C
	L-lactate dehydrogenase A chain (P00338)	UP (1.58)	–	C
	Dehydrogenase/reductase SDR family member 7 (Q9Y394)	UP (1.68)	–	M, N
	Perilipin-2 (Q99541)	DOWN (0.56)	–	PM
Cellular amino acid biosynthetic process (GO:0008652)	Cystathionine gamma-lyase (P32929)	–	UP (1.5)	C
	Ornithine aminotransferase (P04181)	–	UP (1.69)	M
	Asparagine synthetase (P08243)	–	DOWN (0.64)	C
Glutamine metabolic process (GO:0006541)	Argininosuccinate lyase (P04424)	–	UP (1.57)	C, S
	Glutamine-fructose-6-phosphate aminotransferase 1 (Q06210)	–	UP (1.57)	N
	Solute carrier family 2 facilitated glucose transporter member 14 (Q8TDB8)	–	UP (1.9)	PM
	Solute carrier family 2 facilitated glucose transporter member 3 (P11169)	–	UP (1.9)	PM
Glucose transmembrane transport (GO:1904659)				
Inflammation				
Inflammatory response (GO:0006954)	Alpha-1-antitrypsin (P01009)	UP (4.3)	DOWN (0.47)	ER, S
	Haptoglobin (P00738)	UP (4.06)	DOWN (0.27)	S
	Alpha-1-acid glycoprotein 1 (P02763)	UP (6.83)	DOWN (0.27)	S
	Complement C3 (P01024)	UP (2.34)	DOWN (0.47)	S
	Prothrombin (P00734)	UP (2.48)	DOWN (0.4)	S
	Annexin A1 (P04083)	DOWN (0.58)	–	C, N, PM, EN, S
	Phospholipase D3 (Q8IV08)	UP (1.68)	DOWN (0.53)	C, ER, N
	Prostaglandin reductase 1 (Q14914)		UP (1.45)	C

(continued on next page)

Table 1 (continued)

Ontology ID process ¹	Protein name (Uniprot ID)	UP/DOWN (Fold value) ^{1, 2 and 3}		Cell localization
		No treatment	PC treatment	
Positive regulation of inflammatory response (GO:0050729)	Angiotensinogen (P01019)	DOWN (0.62)	DOWN (0.42)	S
Negative regulation of complement activation (GO:0045916)	Plasma protease C1 inhibitor (P05155)	UP (1.92)	DOWN (0.52)	S
	Alpha-2-macroglobulin (P01023)	–	DOWN (0.57)	S
Blood coagulation, common pathway (GO:0072377)	Fibrinogen beta chain (P02675)	UP (1.73)	–	S
	Fibrinogen alpha chain (P02671)	UP (1.61)	–	S
	Fibrinogen gamma chain (P02679)	UP (1.9)	–	S
Positive regulation of wound healing (GO:0090303)	Vitronectin (P04004)	UP (2.33)	DOWN (0.47)	ER
Positive regulation of stress fiber assembly (GO:0051496)	Protein S100-A10 (P60903)	DOWN (0.54)	–	C, ER, PM
Negative regulation of endopeptidase activity (GO:0010951)	Serine protease inhibitor Kazal-type 1 (P00995)	–	DOWN (0.12)	S

List of proteins significantly up-or-downregulated in MMAB1 HLC proteome (compared to C1 healthy HLC) and after PC treatment (compared to non-treated MMAB1 HLC), grouped by their main biological process. Individual information about quantification, Uniprot code and gene ontology (GO) is included.

C: Cytosol; N: Nucleus; ER: Endoplasmic reticulum; S: Secreted; M: Mitochondrion; EN: Endosome; P: Peroxisome; PM: Plasma Membrane.

¹ Official identifier and name of the gene ontology biological process each protein belongs to.

² Fold value represents protein-level dysregulation in MMA *cbIB* HLCs compared to WT HLCs, significantly quantified by PEAKS Studio X Pro software.

³ Tag name for summarizing common biological processes that stands out from proteome data.

also included a dysregulated set of eight DEPs related to chromatin organization, as well as other DEPs involved in hemostasis, including the upregulation of hemopexin and serotransferrin. Finally, oxidative stress dysregulation was noted via increased levels of 6-phosphogluconate dehydrogenase (involved in NADPH generation for reductive power in the cell) and AMBP protein (a precursor of α -1-microglobulin which acts as an antioxidant [54]), and the downregulation of the key enzyme cytosolic superoxide dismutase. Some DEPs were analyzed by western blotting, the results for which is comparable in the MMAB HLCs (which have similar genetic backgrounds), although not in the healthy controls (which do not). Although additional studies with more healthy controls are needed to confirm the liver damage associated with a permanent increase in methylmalonic acid, the present work provides an excellent starting point for determining the potential pathomechanism.

The T3 treatment led to a reduced presence of inflammatory proteins and proteins involved in proteostasis (Table 1). Reductions were also seen in disulfide isomerase and calreticulin, as well as peptidyl-prolyl cis-trans isomerase FKBP10 (involved in correct folding during translation) and ubiquitin. HSP90 alpha protein was, however, upregulated. With respect to the metabolism system, proteins related to lipid biosynthesis such as fatty acid synthase [27] and the cytoplasmic isoform of acetyl-CoA synthase were also upregulated, as was mitochondrial hydroxymethylglutaryl-CoA synthase (involved in the synthesis of ketone bodies [28]) (Supplementary Fig. 2. Increased levels of enzymes involved in cysteine, glutamic acid and proline biosynthesis (such as cystathionine gamma-lyase), the urea cycle enzyme mitochondrial ornithine aminotransferase [29], and cytosolic argininosuccinate lyase (important in increasing urea synthesis and the generation of fumarate for the replenishment of the Krebs cycle) were also seen. No significant modifications were observed for the remaining proteins within the metabolism system. Finally, a reduction was seen in the proteins involved in inflammation (Table 1), including AMBP protein and α -2-macroglobulin (which regulates cytokine signaling induced by oxidative agents [30]). Notably, cytosolic superoxide dismutase, which was downregulated before treatment, was not detected after treatment. In addition, exportin 1 and kinase C (proteins involved in intracellular trafficking [31,32]) were upregulated. No reversion from downregulation was seen for the SNARE or cell structure-related proteins. In summary, the main effect of PC treatment was a significant reduction in

Table 2

Differentially expressed HLC liver proteins (C1 vs MMAB1) before and after pharmacochaperoning treatment.

Protein	Uniprot ID	Gene	UP/DOWN (Fold value)	
			Before PC treatment	After PC treatment
Serum albumin (ALB)	P02768	ALB	UP (2.63)	DOWN (0.23)
Alpha-fetoprotein (AFP)	P02771	AFP	UP (1.77)	DOWN (0.42)
Serotransferrin	P02787	TF	UP (1.48)	DOWN (0.5)
Prothrombin	P00734	F2	UP (2.48)	DOWN (0.4)
Haptoglobin (α -2 HP)	P00738	HP	UP (4.06)	DOWN (0.27)
Alpha-1-antitrypsin (AAT)	P01009	SERPINA1	UP (4.3)	DOWN (0.47)
Angiotensinogen	P01019	AGT	UP (2.73)	DOWN (0.42)
Complement C3	P01024	C3	UP (2.34)	DOWN (0.47)
Alpha-1-acid glycoprotein 1 (AGP)	P02763	ORM1	UP (6.83)	DOWN (0.27)
Phospholipase D3	Q8IV08	PLD3	UP (1.68)	DOWN (0.53)
Annexin A1	P04083	ANXA1	DOWN (0.58)	ND

ND: No differentially expressed.

Individual information about quantification and Uniprot code is included.

Fold value represents protein-level dysregulation in MMA-*cbIB* HLCs compared to control HLCs (before PC treatment), and *cbIB* treated versus non-treated, significantly quantified by PEAKS Studio X Pro software.

both liver damage biomarkers and inflammation response proteins (Table 2).

In summary, this work reports the generation of MMA *cbIB* type HLCs via the reproducible, efficient differentiation of iPSCs, and highlights the potential usefulness of these cells in pharmacological evaluations and cell therapy research.

Supplementary data to this article can be found online at <https://doi.org/10.1016/j.bbdis.2022.166433>.

CRediT authorship contribution statement

Á. Briso-Montiano: Formal analysis, Investigation, Methodology, Writing – original draft. **A. Vilas:** Formal analysis, Investigation, Methodology, Writing – original draft. **E. Richard:** Methodology, Resources, Writing – review & editing. **P. Ruiz-Sala:** Investigation. **E. Morato:** Formal analysis, Investigation. **L.R. Desviat:** Resources, Writing – review & editing. **M. Ugarte:** Resources. **P. Rodríguez-Pombo:** Conceptualization, Funding acquisition, Writing – review & editing. **B. Pérez:** Conceptualization, Funding acquisition, Project administration, Supervision, Writing – original draft.

Declaration of competing interest

The authors declare that they have no known competing financial interests or personal relationships that could have appeared to influence the work reported in this paper.

Acknowledgements

We wholeheartedly thank the Spanish families affected by MMA who actively participated in this research. This work was funded by the *Fundación Isabel Gemio-Fundación La Caixa* [LCF/PR/PR16/11110018], the *Instituto de Salud Carlos III* (ISCIII), European Regional Development Fund [PI19/01155] and the *Consejería de Educación, Juventud y Deporte, Comunidad de Madrid* [B2017/BMD3721].

References

- H.L. Schubert, C.P. Hill, Structure of ATP-bound human ATP:cobalamin adenosyltransferase, *Biochemistry* 45 (2006) 15188–15196, <https://doi.org/10.1021/bi061396f>.
- B. Fowler, J.V. Leonard, M.R. Baumgartner, Causes of and diagnostic approach to methylmalonic acidurias, *J. Inherit. Metab. Dis.* 31 (2008) 350–360, <https://doi.org/10.1007/s10545-008-0839-4>.
- Y. Shigematsu, I. Hata, G. Tajima, Useful second-tier tests in expanded newborn screening of isovaleric acidemia and methylmalonic aciduria, *J. Inherit. Metab. Dis.* 33 (2010) S283–S288, <https://doi.org/10.1007/s10545-010-9111-9>.
- H.A. Haijes, J.J.M. Jans, S.Y. Tas, N.M. Verhoeven-Duif, P.M. van Hasselt, Pathophysiology of propionic and methylmalonic acidemias. Part 1: complications, *J. Inherit. Metab. Dis.* 42 (2019) 730–744, <https://doi.org/10.1002/jimd.12129>.
- P. Forny, M. Hochuli, Y. Rahman, M. Deheragoda, A. Weber, J. Baruteau, et al., Liver neoplasms in methylmalonic aciduria: an emerging complication, *J. Inherit. Metab. Dis.* 42 (2019) 793–802, <https://doi.org/10.1002/jimd.12143>.
- B. Fowler, J.V. Leonard, M.R. Baumgartner, Causes of and diagnostic approach to methylmalonic acidurias, *J. Inherit. Metab. Dis.* 31 (2008) 350–360, <https://doi.org/10.1007/s10545-008-0839-4>.
- P. Forny, F. Hörster, D. Ballhausen, A. Chakrapani, K.A. Chapman, C. Dionisi-Vici, et al., Guidelines for the diagnosis and management of methylmalonic acidemia and propionic acidemia: first revision, *J. Inherit. Metab. Dis.* 44 (2021) 566–592, <https://doi.org/10.1002/jimd.12370>.
- Y.-Z. Jiang, L.-Y. Sun, The value of liver transplantation for methylmalonic acidemia, *Front. Pediatr.* 7 (2019) 87, <https://doi.org/10.3389/fped.2019.00087>.
- A. Gámez, P. Yuste-Checa, S. Brasil, Desviat L.R. Briso-Montiano, M. Ugarte, et al., Protein misfolding diseases: prospects of pharmacological treatment, *Clin. Genet.* 93 (2018) 450–458, <https://doi.org/10.1111/cge.13088>.
- A. Jorge-Finnigan, C. Aguado, R. Sánchez-Alcudia, D. Abia, E. Richard, B. Merinero, et al., Functional and structural analysis of five mutations identified in methylmalonic aciduria cblB type, *Hum. Mutat.* 31 (2010) 1033–1042, <https://doi.org/10.1002/humu.21307>.
- S. Brasil, A. Briso-Montiano, A. Gámez, J. Underhaug, M.I. Flydal, L. Desviat, et al., New perspectives for pharmacological chaperone treatment in methylmalonic aciduria cblB type, *Biochim. Biophys. Acta Mol. basis Dis.* 1864 (2018) 640–648, <https://doi.org/10.1016/j.bbdis.2017.11.024>.
- A. Jorge-Finnigan, S. Brasil, J. Underhaug, P. Ruiz-Sala, B. Merinero, R. Banerjee, et al., Pharmacological chaperones as a potential therapeutic option in methylmalonic aciduria cblB type, *Hum. Mol. Genet.* 22 (2013) 3680–3689, <https://doi.org/10.1093/hmg/ddt217>.
- S.T. Rashid, S. Corbinau, N. Hannan, S.J. Marciniak, E. Miranda, G. Alexander, et al., Modeling inherited metabolic disorders of the liver using human induced pluripotent stem cells, *J. Clin. Invest.* 120 (2010) 3127–3136, <https://doi.org/10.1172/JCI43122>.
- R.G. Rowe, G.Q. Daley, Induced pluripotent stem cells in disease modelling and drug discovery, *Nat Rev Genet* 20 (2019) 377–388, <https://doi.org/10.1038/s41576-019-0100-z>.
- R. Fiorotto, M. Amenduni, V. Mariotti, L. Fabris, C. Spirli, M. Strazzabosco, Liver diseases in the dish: iPSC and organoids as a new approach to modeling liver

- diseases, *Biochim. Biophys. Acta Mol. basis Dis.* 1865 (2019) 920–928, <https://doi.org/10.1016/j.bbdis.2018.08.038>.
- A. Messina, E. Luce, M. Hussein, A. Dubart-Kupperschmitt, Pluripotent-stem-cell-derived hepatic cells: hepatocytes and organoids for liver therapy and regeneration, *Cells* 9 (2020), <https://doi.org/10.3390/cells9020420>.
- T. Yamashita, K. Takayama, M. Hori, M. Harada-Shiba, H. Mizuguchi, Pharmaceutical research for inherited metabolic disorders of the liver using human induced pluripotent stem cell and genome editing technologies, *Biol. Pharm. Bull.* 42 (2019) 312–318, <https://doi.org/10.1248/bpb.b18-00544>.
- E. Pareja, M.J. Gómez-Lechón, L. Tolosa, Induced pluripotent stem cells for the treatment of liver diseases: challenges and perspectives from a clinical viewpoint, *Ann. Transl. Med.* 8 (2020) 566, <https://doi.org/10.21037/atm.2020.02.164>.
- Y. Wang, S. Alhaque, K. Cameron, J. Meseguer-Ripolles, B. Lucendo-Villarin, H. Rashidi, et al., Defined and scalable generation of hepatocyte-like cells from human pluripotent stem cells, *J. Vis. Exp.* (2017), <https://doi.org/10.3791/55355>.
- A. Imbard, N. Garcia Segarra, M. Tardieu, P. Broué, J. Bouchereau, S. Pichard, et al., Long-term liver disease in methylmalonic and propionic acidemias, *Mol. Genet. Metab.* 123 (2018) 433–440, <https://doi.org/10.1016/j.ymgme.2018.01.009>.
- E. Richard, S. Brasil, A. Briso-Montiano, E. Alonso-Barroso, M.E. Gallardo, B. Merinero, et al., Generation and characterization of two human iPSC lines from patients with methylmalonic acidemia cblB type, *Stem Cell Res.* 29 (2018) 143–147, <https://doi.org/10.1016/j.scr.2018.03.021>.
- L.L. Torres, A. Cantero, M. del Valle, A. Marina, F. López-Gallego, J.M. Guisán, et al., Engineering the substrate specificity of a thermophilic penicillin acylase from *thermus thermophilus*, *Appl. Environ. Microbiol.* 79 (2013) 1555–1562, <https://doi.org/10.1128/AEM.03215-12>.
- X. Zhou, W. Xiao, Z. Su, J. Cheng, C. Zheng, Z. Zhang, et al., Hippocampal proteomic alteration in triple transgenic mouse model of Alzheimer's disease and implication of PINK 1 regulation in donepezil treatment, *J. Proteome Res.* 18 (2019) 1542–1552, <https://doi.org/10.1021/acs.jproteome.8b00818>.
- H. Suárez, Z. Andreu, C. Mazzeo, V. Toribio, A.E. Pérez-Rivera, S. López-Martín, et al., CD9 inhibition reveals a functional connection of extracellular vesicle secretion with mitophagy in melanoma cells, *J. Extracell. Vesicles* 10 (2021), e12082, <https://doi.org/10.1002/jev2.12082>.
- T. Hurrell, C.-P. Segeritz, L. Vallier, K.S. Lilley, A.D. Cromarty, A proteomic time course through the differentiation of human induced pluripotent stem cells into hepatocyte-like cells, *Sci. Rep.* 9 (2019) 3270, <https://doi.org/10.1038/s41598-019-39400-1>.
- H.J. Blom, A. van Rooij, M. Hogeveen, A simple high-throughput method for the determination of plasma methylmalonic acid by liquid chromatography-tandem mass spectrometry, *Clin. Chem. Lab. Med.* 45 (2007) 645–650, <https://doi.org/10.1515/CCLM.2007.117>.
- M.S. Choi, J.-Y. Jung, H.-J. Kim, M.R. Ham, T.R. Lee, D.W. Shin, S-nitrosylation of fatty acid synthase regulates its activity through dimerization, *J. Lipid Res.* 57 (2016) 607–615, <https://doi.org/10.1194/jlr.M065805>.
- B. Puiasc, I. Marcos-Alcalde, M. Hernández-Marcos, P. Tobajas Morlana, A. Levitova, B.C. Schwahn, et al., Human mitochondrial HMG-CoA synthase deficiency: role of enzyme dimerization surface and characterization of three new patients, *Int. J. Mol. Sci.* 19 (2018) E1010, <https://doi.org/10.3390/ijms19041010>.
- A. Ginguay, L. Cynober, E. Curis, I. Nicolis, Ornithine aminotransferase, an important glutamate-metabolizing enzyme at the crossroads of multiple metabolic pathways, *Biology (Basel)* 6 (2017) E18, <https://doi.org/10.3390/biology6010018>.
- J.H. Cater, M.R. Wilson, A.R. Wyatt, Alpha-2-macroglobulin, a hypochlorite-regulated chaperone and immune system modulator, *Oxidative Med. Cell. Longev.* 2019 (2019) 5410657, <https://doi.org/10.1155/2019/5410657>.
- B. Ossareh-Nazari, F. Bachelier, C. Dargemont, Evidence for a role of CRM1 in signal-mediated nuclear protein export, *Science* 278 (1997) 141–144, <https://doi.org/10.1126/science.278.5335.141>.
- W. Roach, M. Plomann, PACSIN3 overexpression increases adipocyte glucose transport through GLUT1, *Biochem. Biophys. Res. Commun.* 355 (2007) 745–750, <https://doi.org/10.1016/j.bbrc.2007.02.025>.
- X. Xu, Z. Zhong, Disease modeling and drug screening for neurological diseases using human induced pluripotent stem cells, *Acta Pharmacol. Sin.* 34 (2013) 755–764, <https://doi.org/10.1038/aps.2013.63>.
- M. Zabulica, T. Jakobsson, F. Ravaioli, M. Vosough, R. Gramignoli, E. Ellis, et al., Gene editing correction of a urea cycle defect in organoid stem cell derived hepatocyte-like cells, *Int. J. Mol. Sci.* 22 (2021) 1217, <https://doi.org/10.3390/ijms22031217>.
- T. Takebe, K. Sekine, M. Enomura, H. Koike, M. Kimura, T. Ogaeri, et al., Vascularized and functional human liver from an iPSC-derived organ bud transplant, *Nature* 499 (2013) 481–484, <https://doi.org/10.1038/nature12271>.
- T. Schwander, J. McLean, J. Zarzycki, T.J. Erb, Structural basis for substrate specificity of methylsuccinyl-CoA dehydrogenase, an unusual member of the acyl-CoA dehydrogenase family, *J. Biol. Chem.* 293 (2018) 1702–1712, <https://doi.org/10.1074/jbc.RA117.000764>.
- D. Oaxaca-Castillo, P. Andreoletti, A. Vluggens, S. Yu, P.P. van Veldhoven, J. K. Reddy, et al., Biochemical characterization of two functional human liver acyl-CoA oxidase isoforms 1a and 1b encoded by a single gene, *Biochem. Biophys. Res. Commun.* 360 (2007) 314–319, <https://doi.org/10.1016/j.bbrc.2007.06.059>.
- H.Q. Smith, C. Li, C.A. Stanley, T.J. Smith, Glutamate dehydrogenase, a complex enzyme at a crucial metabolic branch point, *Neurochem. Res.* 44 (2019) 117–132, <https://doi.org/10.1007/s11064-017-2428-0>.
- M. Caterino, R.J. Chandler, J.L. Sloan, K. Dorko, K. Cusmano-Ozog, L. Ingenito, et al., The proteome of methylmalonic acidemia (MMA): the elucidation of altered

- pathways in patient livers, *Mol. BioSyst.* 12 (2016) 566–574, <https://doi.org/10.1039/c5mb00736d>.
- [40] C. Gabay, I. Kushner, Acute-phase proteins and other systemic responses to inflammation, *N. Engl. J. Med.* 340 (1999) 448–454, <https://doi.org/10.1056/NEJM199902113400607>.
- [41] W. Schrödl, R. Büchler, S. Wendler, P. Reinhold, P. Muckova, J. Reindl, et al., Acute phase proteins as promising biomarkers: perspectives and limitations for human and veterinary medicine, *Proteomics Clin Appl* 10 (2016) 1077–1092, <https://doi.org/10.1002/prca.201600028>.
- [46] P.-L. Lee, K.-Y. Lee, T.-M. Cheng, H.-C. Chuang, S.-M. Wu, P.-H. Feng, et al., Relationships of haptoglobin phenotypes with systemic inflammation and the severity of chronic obstructive pulmonary disease, *Sci. Rep.* 9 (2019) 189, <https://doi.org/10.1038/s41598-018-37406-9>.
- [47] K. Göbel, S. Eichler, H. Wiendl, T. Chavakis, C. Kleinschnitz, S.G. Meuth, The coagulation factors fibrinogen, thrombin, and factor XII in inflammatory disorders—a systematic review, *Front. Immunol.* 9 (2018) 1731, <https://doi.org/10.3389/fimmu.2018.01731>.
- [48] J. Mesa, C. Alsina, U. Oppermann, X. Parés, J. Farrés, S. Porté, Human prostaglandin reductase 1 (PGR1): substrate specificity, inhibitor analysis and site-directed mutagenesis, *Chem. Biol. Interact.* 234 (2015) 105–113, <https://doi.org/10.1016/j.cbi.2015.01.021>.
- [49] P.-F. Han, X.-D. Che, H.-Z. Li, Y.-Y. Gao, X.-C. Wei, P.-C. Li, Annexin A1 involved in the regulation of inflammation and cell signaling pathways, *Chin. J. Traumatol.* 23 (2020) 96–101, <https://doi.org/10.1016/j.cjtee.2020.02.002>.
- [50] S. Thibeaux, S. Siddiqi, O. Zhelyabovska, F. Moinuddin, M.M. Masternak, S. A. Siddiqi, Cathepsin B regulates hepatic lipid metabolism by cleaving liver fatty acid-binding protein, *J. Biol. Chem.* 293 (2018) 1910–1923, <https://doi.org/10.1074/jbc.M117.778365>.
- [51] X. Zhou, L. Sun, O. Bracko, J.W. Choi, Y. Jia, A.L. Nana, et al., Impaired prosaposin lysosomal trafficking in frontotemporal lobar degeneration due to progranulin mutations, *Nat. Commun.* 8 (2017) 15277, <https://doi.org/10.1038/ncomms15277>.
- [52] R.J. McKenney, W. Huynh, M.E. Tanenbaum, G. Bhabha, R.D. Vale, Activation of cytoplasmic dynein motility by dynactin-cargo adapter complexes, *Science* 345 (2014) 337–341, <https://doi.org/10.1126/science.1254198>.
- [53] M. Costanzo, M. Caterino, A. Cevenini, V. Jung, C. Chhuon, J. Lipecka, et al., Proteomics reveals that methylmalonyl-CoA mutase modulates cell architecture and increases susceptibility to stress, *Int. J. Mol. Sci.* 21 (2020) E4998, <https://doi.org/10.3390/ijms21144998>.
- [54] R.A. Zager, Alpha 1 microglobulin: a potentially paradoxical anti-oxidant agent, *Adv. Tech. Biol. Med.* 5 (2017) 238, <https://doi.org/10.4172/2379-1764.1000238>.